JACS
JOURNAL OF THE AMERICAN CHEMICAL SOCIETY
Communication
pubs.acs.org/JACS

Electrochemiluminescence Tuned by Electron−Hole Recombination from Symmetry-Breaking in Wurtzite ZnSe

Suli Liu,[†,∥] Qinghua Zhang,[‡,∥] Long Zhang,[†] Lin Gu,[‡] Guizheng Zou,[§] Jianchun Bao,[†] and Zhihui Dai*[,†]

[†]Jiangsu Collaborative Innovation Center of Biomedical Functional Materials and Jiangsu Key Laboratory of Biofunctional Materials, School of Chemistry and Materials Science, Nanjing Normal University, Nanjing 210023, P. R. China

[‡]Beijing National Laboratory for Condensed Matter Physics, Institute of Physics, Chinese Academy of Sciences, Beijing 100190, P. R. China

[§]School of Chemistry and Chemical Engineering, Shandong University, Jinan 250100, P. R. China

Supporting Information

ABSTRACT: The research of highly active electrochemiluminescence (ECL) materials with low toxicity and good solubility remains a substantial challenge. In this work, we present a synthesis method to prepare soluble wurtzite (WZ) ZnSe nanocrystals (NCs), which exhibit good ECL properties. Using high-angle annular-dark-field imaging together with electron hologram methods, we observe that the WZ ZnSe NCs exhibit an unusual symmetry-breaking phenomenon, where the translational symmetry of the polarized Zn−Se bond is broken. The formation of a symmetry-breaking region leads to an accumulation of charge. The good ECL response originates from the increased efficiency of electron−hole recombination by the excess charge redistribution in WZ ZnSe NCs. This study of the relationship between ECL behavior and the architecture of NCs suggests that careful control over the NC structures of semiconductors can tailor their charge distribution via symmetry breaking, which opens new avenues for the design of novel classes of agents for optoelectronic applications.

In recent years, an increasing number of semiconductor nanocrystals (NCs) have been exploited as electrochemiluminescence (ECL) reagents.[1−5] The ECL behaviors of Si, Ge, and SiO_2 in an organic solvent have been reported. Although ECL features were observed in these systems, they exhibited low ECL intensities. Some heavy-metal-containing semiconductor NCs (CdSe or PbSe) can produce ECL; however, they released Cd^{2+} or Pb^{2+} ions, which were highly cytotoxic and lead to serious health and environmental concerns.[4,6,7] Thus, core−shell-structured NCs such as CdSe@ZnSe,[4] CdTe@SiO_2,[6] and CdS@ZnO[7] have been synthesized by capping NCs with environmentally friendly materials to prevent the leakage of toxic ions. Nevertheless, ECL properties of core−shell NCs were limited due to their complicated synthesis. Thus, the facile synthesis of highly active ECL reagents with low toxicity and good solubility remains a substantial challenge. Traditionally, ECL generated from semiconductor NCs has suggested the potential for charge-transfer reactions either at band edges or at interfaces with passivated surfaces.[4,8−11] In brief, nonpassivated surface atoms can form electronic traps for electrons and holes, and these traps affect luminescence processes. When an electron is injected into a surface trap within the band gap of the NC, ECL emission with a substantial red shift relative to the photoluminescence (PL) emission can be induced.[12] The ECL emission from such NCs (e.g., Si[10] and CdSe[1]) has been attributed to an electron-transfer reaction. However, when the surface of the NC is passivated with a shell, the injected electron can return to the valence band. In these cases, the resultant ECL spectrum resembles the PL spectrum.[12] The ECL emission from CdSe/ZnSe NCs has been attributed to the surface passivation of the CdSe NCs.[4] However, up to now, there is no report concerning the ECL mechanism with characteristics of NC semiconductor architecture, charge distribution, and electron−hole recombination.

As a typical representative of II−VI semiconductor NCs, ZnSe possesses structures that include zincblende (ZB), with cubic stacking in the [111] direction, and wurtzite (WZ), with hexagonal stacking in the [0001] direction.[13−16] ZB ZnSe is thermodynamically stable, whereas WZ ZnSe is metastable. In comparison with ZB ZnSe, WZ ZnSe is difficult to prepare under mild reaction conditions.[17,18] Furthermore, the controlled growth of WZ ZnSe NCs with alternating Zn and Se atom arrangements leads to a localized excess of charge, which is due to the polarization associated with symmetry-breaking structures.[15,16,19] The accumulation of charge in the WZ ZnSe structure can also affect the electron−hole recombination statistics, which may result in new properties.[20,21] Here, we propose WZ ZnSe as an ideal model to investigate the relationship between the WZ ZnSe structure and its ECL behavior.

In this study, we develop a facile method to prepare WZ ZnSe NCs with symmetry-breaking structures and good solubility by using terpineol as a reducing agent and capping reagent. Furthermore, high-angle annular-dark-field (HAADF) imaging together with an electron hologram experiment is employed to gain insight into the structural features of the WZ ZnSe NCs. The WZ ZnSe NCs exhibit an unusual symmetry-breaking phenomenon, where the translational symmetry of the polarized Zn−Se bond is disrupted. This phenomenon leads to a region of charge accumulation. At the same time, the WZ

Received: December 5, 2015
Published: January 19, 2016

DOI: 10.1021/jacs.5b12727
J. Am. Chem. Soc. 2016, 138, 1154−1157

ZnSe NCs exhibit good ECL properties in an aqueous solution, outperforming ZB ZnSe NCs and bulk ZnSe. Experimental measurements reveal that the ECL response originates from an increased efficiency in electron−hole recombination because of a redistribution of the excess charge in WZ ZnSe NCs. The results of this study suggest that, through careful control of semiconductor crystal structure, the redistribution of charge redistributions can be tailored via symmetry-breaking, which creates the novel ECL materials.

Transmission electron microscopy (TEM) images reveal that the size of the as-synthesized WZ ZnSe NCs is ∼15 nm (Figure S1a). A typical X-ray diffraction (XRD) pattern for these particles is shown in Figure S1b and exhibits sharp diffraction peaks that are indexed as the (100), (002), (101), (102), (210), (103), and (200) planes of WZ ZnSe (JCPDS Card No. 80-08). Raman spectroscopy is used to further characterize this phase (Figure S1c). The Raman spectra of WZ ZnSe NCs contain peaks at 201 and 249 cm^{-1} that arise from the transverse optical (TO) and longitudinal optical (LO) phonons of ZnSe.[22] The LO phonon of the WZ ZnSe NCs is slightly blue-shifted compared with that of the ZB ZnSe NCs. Furthermore, the peak at 174 cm^{-1} can only be observed in WZ ZnSe NCs.[22] Extensive studies employing X-ray photoelectron spectroscopy (XPS) are conducted to explore the surface properties of elements (e.g., the bonding of surface atoms and their electronic structure) in WZ ZnSe. As illustrated in Figure S1d, the Zn 2p core-level spectra (Zn $2p_{3/2}$ and $2p_{1/2}$) are symmetric, narrow, and devoid of satellite peaks, which indicates that the valence state of Zn is +2 for both the WZ and ZB ZnSe NCs.[14] In the case of the WZ ZnSe NCs, the binding energies (BEs) of Zn $2p_{3/2}$ and Zn $2p_{1/2}$ are 1022 and 1045 eV, respectively, which are slightly higher than those of ZB ZnSe NCs. In the case of the Se 3d spectra, only a single broad peak located at 52−56 eV is observed for these two samples (Figure S1e). The shapes of these peaks are characteristic of Se^{2-} in a uniform bonding environment.[12] The broad peaks for Se 3d are fitted with two symmetric peaks assigned to Se $3d_{5/2}$ and Se $3d_{3/2}$ (Figures S1f and S1g). Similar to the Zn 2p spectra, the BEs of the Se $3d_{5/2}$ and the Se $3d_{3/2}$ peaks for WZ ZnSe NCs are slightly higher than those of ZB ZnSe NCs. The slight differences in BEs observed in the Zn 2p and Se 3d peaks in the spectra of WZ and ZB ZnSe NCs confirm that the arrangement of their surface atoms or their electronic structures are distinct, which may lead to diverse ECL properties.[23]

The atomic arrangement for the surface of WZ ZnSe NCs is presented in Figure 1. As evident from the normal WZ ZnSe shown in Figure 1a, the projected orientation of the Zn−Se bonds in the horizontal direction are reversed in alternating rows along the *c*-axis (indicated by red and green arrows). This orientation indicates that the spontaneous polarization is aligned with the *c*-direction, without a component in the *ab* plane, and corresponds to its polarized space group *P*63*mc*.[15,20] In our case, however, we observe an unusual symmetry-breaking structure and polarization phenomenon with the WZ ZnSe NCs. Figure 1b is the HAADF image of a typical WZ ZnSe particle that contains defective segments. On the basis of the Z-contrast mechanism of the HAADF image, where intensity is highly sensitive to atomic number Z and is approximately proportional to Z^2, we identify the brighter dots as Se atoms.[15] To clarify the image, we superimpose a structural model of WZ ZnSe in the upper left corner of Figure 1b and place the simulated HAADF image at the bottom right corner. Consequently, the atomic arrangement for the experimental

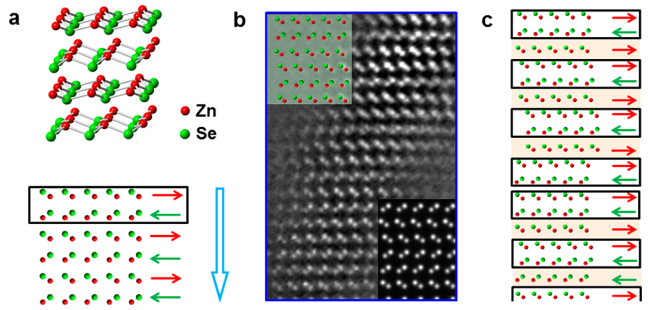

Figure 1. (a) Structure model of WZ ZnSe (upper part) and its projection along the [100] direction (lower part). The directing of the Zn−Se bond is indicated by red and green arrows in the horizontal direction. (b) Aberration-corrected HAADF image of WZ ZnSe containing symmetry-breaking defects. Structure model is overlapped at the upper left corner; simulated HAADF image at the bottom right corner. (c) Atomic structure corresponding to (b); the projected directing of the Zn−Se bond is also indicated by green and red arrows.

image is obtained, which is shown in Figure 1c. The projected directions of the Zn−Se bonds are also indicated by green and red arrows. To highlight the charge accumulation in WZ ZnSe NCs, black rectangles to horizontally frame neutral units in the *ab* plane are used. Clearly, several layers with an unpaired horizontal polarization are present, which are identified by the light colored background. As a result, the translational symmetry-breaking of the Zn−Se bonding introduces a net charge.

To characterize the charge state of WZ ZnSe with greater confidence, we perform electron hologram experiments. A symmetry-breaking phenomenon with blurred contrast in the center of the WZ ZnSe particle is clearly evident in the high-resolution transmission electron microscopy (HRTEM) image in Figure 2a. This phenomenon corresponds to the defect region in the HAADF image of Figure 1b. The complex image (Figure 2b), consisting of the amplitude and the phase of the electron wave, is reconstructed using the holowork package. The resultant phase image is separated from the reconstructed complex image and is shown in Figure 2c. According to the theory of electron holography, the phase shift of the incident

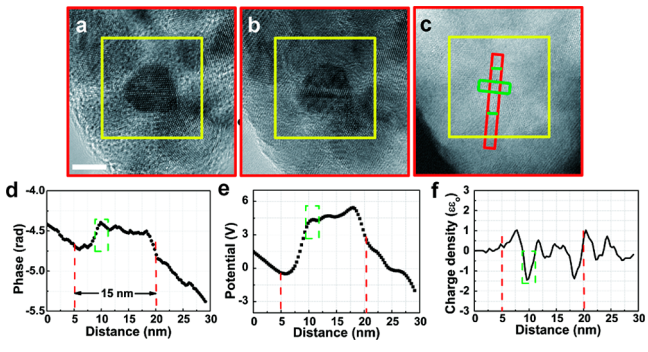

Figure 2. (a) HRTEM image along the [100] direction of a ZnSe particle that contains a symmetry-breaking region. Scale bar is 10 nm. (b and c) The hologram and reconstructed phase diagram of (a), respectively. (d, e, and f) Line profiles associated with the phase, the potential and the charge density, respectively, as indicated by the red rectangle in (c). The green-dotted rectangles in (c)−(f) outline the position of the polarity defect, and the two green lines in (c) mark the edges of the particle. The two red-dotted lines in (d)−(f) indicate the edges of the ZnSe particle.

DOI: 10.1021/jacs.5b12727
J. Am. Chem. Soc. 2016, 138, 1154−1157

electron beam is proportional to the electrostatic field of a sample with nearly constant thickness. Here, the thickness effect is ignored because of the small size of our NCs. Figure 2d is the phase profile extracted along the [100] direction, indicated by the red rectangle in Figure 2c. It shows the obvious phase variation around the ZnSe particle. The phase value is determined to be high at the position of the polarized defect. To obtain the origin of this phase shift, the potential profile (Figure 2e) and the charge density profile (Figure 2f) are extracted from Figure 2d using holograph theory. A potential difference of 0.5 V and a peak charge density of $-1.5\ \varepsilon\varepsilon_o$ are determined and indicated by the green-dotted rectangles in Figures 2e and 2f, respectively. Thus, negative charges indeed exist at the region of broken translational symmetry.

Semiconductor NCs are typically synthesized in organic solution with oleylamine.[24,25] The oleylamine capping the surface of NCs has effects on the solubility of the NCs. It needs to be additionally "cleaned" (e.g., acid or base treatment, and ligand exchange with small adsorbates) when used in an aqueous solution.[25] In the present case, besides replacing toxic alkylphosphines, which can reduce SeO_2 to Se(-II), the terpineol increases the solubility of the WZ ZnSe NCs (Figure S2). Thus, the obtained WZ ZnSe NCs can be directly utilized without the need for extra treatment. This new, easy, and effective method greatly benefits the development of ECL semiconductor NCs.

The ECL behaviors of the obtained WZ ZnSe NCs are studied. Figure 3a shows the ECL spectrum of an electrode

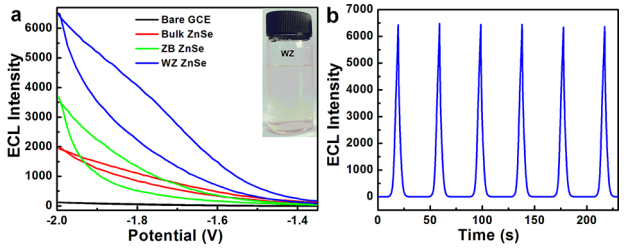

Figure 3. (a) ECL intensity of bare GCE (black line), bulk ZnSe (red line), ZB ZnSe (green line), and WZ ZnSe (blue line) modified electrodes after surface modification in a 0.1 M KOH containing 0.1 M $K_2S_2O_8$ solution (n = 3). Scan rate: 100 mV s^{-1} (inset: photograph showing the good solubility of the WZ ZnSe). (b) Stability of ECL emissions from the WZ ZnSe-modified GCE during six cycles of continuous CV scans in a 0.1 M KOH containing 0.1 M $K_2S_2O_8$ solution (n = 3).

modified with WZ ZnSe (blue line) in 0.1 M KOH, between −1.35 and −2.0 V, at a scan rate of 100 mV s^{-1} and in the presence of 0.1 M $K_2S_2O_8$ as a coreactant. For comparison, the ECL spectra under the same experimental conditions for bare glassy carbon electrode (GCE) (black line), ZB ZnSe (green line), and bulk ZnSe (red line) modified electrodes are also included in Figure 3a. The WZ ZnSe modified electrode exhibits intense ECL emissions, with onset potentials at approximately −1.35 V. These emissions are substantially more intense than the background signal. Notably, the ECL intensity of the WZ ZnSe NCs is greater than those of other ZnSe NCs, indicating that the WZ ZnSe NCs dramatically enhance the ECL activity.[5] In addition to ECL intensity, long-term stability or durability is another important parameter. Figure 3b displays the ECL emission of the WZ ZnSe modified GCE for six cycles of continuous potential scans. Stable ECL signals with a relative standard deviation of 0.36% are observed, which indicates the WZ ZnSe NCs can be used as an ECL sensor. Additionally, the stability of ZB ZnSe NCs is also shown in Figure S3. It can be seen that the stability of ZB ZnSe NCs is acceptable.

It was reported that some methods were designed to change the surface charge or structure of NCs by chemical or physical interactions between analytes and semiconductor NCs, which can also affect the efficiency of the core electron−hole recombination and thus the luminescent emission.[5,26,27] On the basis of this work, the relative ECL intensities of the studied materials increase in the order bare < bulk ZnSe < ZB ZnSe < WZ ZnSe modified GCEs. In general, the bulk ZnSe crystal is the most stable.[17,28,29] The characterizations of bulk ZnSe have been shown in Figure S4. In addition, we also perform detailed structural characterizations for ZB ZnSe NCs that contain symmetry-breaking, as displayed in Figures S5, S6, and S7, respectively. Two symmetry-breaking defects are clearly evident in the particle, as outlined by the yellow frame in Figure S6a. The complex image (Figure S6b) consists of the amplitude and the phase of the electron wave, which are reconstructed using the holowork package. The corresponding phase image is separated from the reconstructed complex image, which is shown in Figure S6c. Figure S6d is the phase profile extracted along the direction indicated by the red rectangle. It shows the observable phase variation around the ZB ZnSe particle with the symmetry-breakings. The phase value is detected as high at the positions associated with symmetry-breaking. The potential profile (Figure S6e) and the charge-density profile (Figure S6f) are also extracted from Figure S6d. Two potential differences of 1.13 and 0.95 V, which correspond to charge-density peaks of $-0.35\ \varepsilon\varepsilon_o$ and $0.18\ \varepsilon\varepsilon_o$, respectively, are indicated by the green-dotted rectangle, as shown in Figure S6f. However, the WZ ZnSe NCs exhibit an unusual symmetry-breaking phenomenon, where the amount of charge accumulated apparently differs from that observed in the ZB ZnSe NCs. On the basis of the aforementioned structural characterizations and ECL activity, the charge-density peaks of ZnSe NCs increase in the order bare < bulk ZnSe < ZB ZnSe < WZ ZnSe modified GCEs. The level of improvement in ECL activity is consistent with this trend. According to the previous reports,[1,2,5,8] it can be speculated that the negative net charge is injected to the conduction band of the ZnSe NCs to produce the negatively charged ZnSe ($ZnSe^{\bullet-}$). Then, reduction of the $S_2O_8^{2-}$ produces a strong oxidant ($SO_4^{\bullet-}$). With the increased net charge from $0.18\ \varepsilon\varepsilon_o$ or $-0.35\ \varepsilon\varepsilon_o$ to $-1.5\ \varepsilon\varepsilon_o$, more ZnSe* is produced from oxidation of the $ZnSe^{\bullet-}$ by the electrogenerated $SO_4^{\bullet-}$. Finally, ZnSe* decays back to the ground state ZnSe accompanied by the light emission, leading to a remarkable difference in the ECL intensity.

Figure 4 indicates that the maximum ECL emission wavelength (793 nm) of WZ ZnSe NCs is substantially red-shifted 368 nm from the PL maximum (425 nm). While the maximum ECL emission wavelength of ZB ZnSe NCs is red-shifted 344 nm compared to the PL spectrum (Figure S8). These distinct differences in the amount of red shift observed for WZ and ZB ZnSe NCs are attributed to a surface effect because of the difference in the amount of charge accumulated for the WZ and ZB ZnSe NCs, and the amount of red shift depends on the degree of symmetry-breaking.

Consequently, the ECL mechanism of the ZnSe NCs has been proposed to involve the formation of an excited-state ZnSe* and the strongly oxidizing $SO_4^{\bullet-}$ radicals produced by

DOI: 10.1021/jacs.5b12727
J. Am. Chem. Soc. 2016, 138, 1154−1157

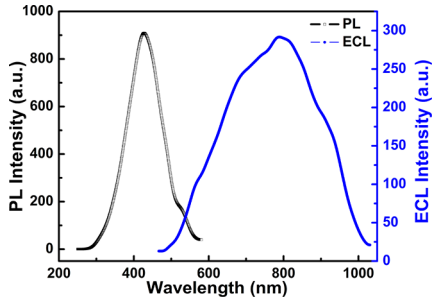

Figure 4. PL spectrum of WZ ZnSe NCs and ECL spectrum of the WZ ZnSe in a 0.1 M KOH containing 0.1 M $K_2S_2O_8$ solution.

the electroreduction of $S_2O_8^{2-}$, as shown in Figure 5.[1−5,30,31] On the basis of our results, we suggest that the negative net charge effectively motivates the luminescence of WZ ZnSe NCs by enhancing the efficiency of electron−hole recombination.

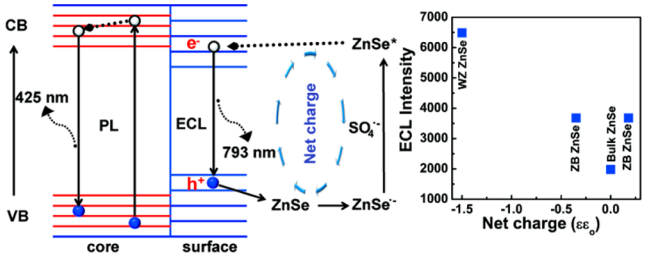

Figure 5. Scheme of the ECL mechanism in WZ ZnSe NCs. $ZnSe^{\bullet-}$ and ZnSe* represent negatively charged and excited-state WZ ZnSe NCs, respectively.

In conclusion, WZ ZnSe NCs with symmetry-breaking structures and good solubility are prepared by a simple chemical route and subsequently exhibit greater ECL activity than those of other ZnSe NCs. On the basis of the results presented herein, we propose a mechanism to explain the ECL performance variations caused by electron−hole recombination and demonstrate the feasibility of tailoring the charge distribution in WZ ZnSe NCs. The findings of this work can be used to predict the optimal structure for good ECL activity and to guide the synthetic control of defect structures in semiconductor NCs via the relationship between an excess of negative charges in WZ ZnSe NCs and the obtained ECL performance.

■ ASSOCIATED CONTENT

Supporting Information

The Supporting Information is available free of charge on the ACS Publications website at DOI: 10.1021/jacs.5b12727.

Details of experiments, structural characterizations, and PL-ECL data (PDF)

■ AUTHOR INFORMATION

Corresponding Author

*daizhihuii@njnu.edu.cn

Author Contributions

‖S.L. and Q.Z. contributed equally.

Notes

The authors declare no competing financial interest.

■ ACKNOWLEDGMENTS

We thank the financial support from the NSFC (Nos. 21175069, 21471081, 21475062, 21427808, and 51332001), Strategic Priority Research Program of the Chinese Academy of Sciences (Grant No. XDB07030200), and PAPD.

■ REFERENCES

(1) Liu, Z. Y.; Qi, W. J.; Xu, G. B. *Chem. Soc. Rev.* **2015**, *44*, 3117.
(2) Wu, P.; Hou, X. D.; Xu, J. J.; Chen, H. Y. *Chem. Rev.* **2014**, *114*, 11027.
(3) Hesari, M.; Swanick, K. N.; Lu, J. S.; Whyte, R.; Wang, S. N.; Ding, Z. F. *J. Am. Chem. Soc.* **2015**, *137*, 11266.
(4) Myung, N.; Bae, Y.; Bard, A. J. *Nano Lett.* **2003**, *3*, 1053.
(5) Zheng, L. Y.; Chi, Y. W.; Dong, Y. Q.; Lin, J. P.; Wang, B. B. *J. Am. Chem. Soc.* **2009**, *131*, 4564.
(6) Wei, W.; Zhou, J.; Li, H. N.; Yin, L. H.; Pu, Y. P.; Liu, S. Q. *Analyst* **2013**, *138*, 3253.
(7) Liu, D. Q.; Wang, L.; Ma, S. H.; Jiang, Z. H.; Yang, B.; Han, X. J.; Liu, S. Q. *Nanoscale* **2015**, *7*, 3627.
(8) Ding, Z. F.; Quinn, B. M.; Haram, S. K.; Pell, L. E.; Korgel, B. A.; Bard, A. J. *Science* **2002**, *296*, 1293.
(9) Hesari, M.; Swanick, K. N.; Lu, J. S.; Whyte, R.; Wang, S.; Ding, Z. F. *J. Am. Chem. Soc.* **2015**, *137*, 11266.
(10) Zhang, X. D.; Chen, X. K.; Kai, S. Q.; Wang, H. Y.; Yang, J. J.; Wu, F. G.; Chen, Z. *Anal. Chem.* **2015**, *87*, 3360.
(11) Yam, V. W. W.; Au, V. K. M.; Leung, S. Y. L. *Chem. Rev.* **2015**, *115*, 7589.
(12) Miao, W. J. *Chem. Rev.* **2008**, *108*, 2506.
(13) Wang, S. T.; Feng, G. Y.; Zhou, S. *Appl. Phys. Lett.* **2014**, *105*, 253110.
(14) Chen, P.; Xiao, T. Y.; Li, H. H.; Yang, J. J.; Wang, Z.; Yao, H. B.; Yu, S. H. *ACS Nano* **2012**, *6*, 712.
(15) Li, L. Y.; Tu, F. F.; Jin, L.; Choy, W. C. H.; Gao, Y. H.; Wang, J. B. *Sci. Rep.* **2014**, *4*, 7447.
(16) Xu, J.; Wang, C. R.; Wu, B. H.; Xu, X. F.; Chen, X. S.; Oh, H.; Baek, H.; Yi, G. C. *J. Appl. Phys.* **2014**, *116*, 174303.
(17) Dawood, F.; Schaak, R. E. *J. Am. Chem. Soc.* **2009**, *131*, 424.
(18) Li, H. B.; Zanella, M.; Genovese, A.; Povia, M.; Falqui, A.; Giannini, C.; Manna, L. *Nano Lett.* **2011**, *11*, 4964.
(19) Liu, M. K.; Powell, D. A.; Shadrivov, I. V.; Lapine, M.; Kivshar, Y. S. *Nat. Commun.* **2014**, *5*, 4441.
(20) Li, L. Y.; Jin, L.; Wang, J. B.; Smith, D. J.; Yin, W. J.; Yan, Y. F.; Sang, H. Q.; Choy, W. C. H.; McCartney, M. R. *Adv. Mater.* **2012**, *24*, 1328.
(21) Yang, S.; Ni, X. J.; Yin, X. B.; Kante, B.; Zhang, P.; Zhu, J.; Wang, Y.; Zhang, X. *Nat. Nanotechnol.* **2014**, *9*, 1002.
(22) Sparks, J. R.; He, R.; Healy, N.; Krishnamurthi, M.; Peacock, A. C.; Sazio, P. J.; Gopalan, V.; Badding, J. V. *Adv. Mater.* **2011**, *23*, 1647.
(23) Liu, S. L.; Zhang, Q. H.; Li, Y. F.; Han, M.; Gu, L.; Nan, C. W.; Bao, J. C.; Dai, Z. H. *J. Am. Chem. Soc.* **2015**, *137*, 2820.
(24) Mazumder, V.; Sun, S. H. *J. Am. Chem. Soc.* **2009**, *131*, 4588.
(25) Niu, Z. Q.; Li, Y. D. *Chem. Mater.* **2014**, *26*, 72.
(26) Jin, L. H.; Han, C. S. *Anal. Chem.* **2014**, *86*, 7209.
(27) Liu, X.; Jiang, H.; Lei, J. P.; Ju, H. X. *Anal. Chem.* **2007**, *79*, 8055.
(28) Wang, H.; Yuan, H.; Hong, S. S.; Li, Y.; Cui, Y. *Chem. Soc. Rev.* **2015**, *44*, 2664.
(29) Sun, Y. F.; Gao, S.; Lei, F. C.; Xie, Y. *Chem. Soc. Rev.* **2015**, *44*, 623.
(30) Wang, J.; Han, H. Y.; Jiang, X. C.; Huang, L.; Chen, L. N.; Li, N. *Anal. Chem.* **2012**, *84*, 4893.
(31) Zhu, C. Z.; Yang, G. H.; Li, H.; Du, D.; Lin, Y. H. *Anal. Chem.* **2015**, *87*, 230.

DOI: 10.1021/jacs.5b12727
J. Am. Chem. Soc. 2016, 138, 1154−1157